Highly Sensitive Mutual-Capacitive Fingerprint Sensor With Reference Electrode

Junghoon Yang, Yeon-Wha Oh, Sarawut Siracosit, Hyunwoo Park, Jungmoo Lee, Sang Gyun Kim, Hanbyul Kim, Kyunghak Lee, Guk-Jin Jeon, Jae-Hyun Ahn, Sang-Hee Jung, Il-Suk Kang, and Sang-Hee Ko Park

***Abstract*— The sensitivity of existing fingerprint sensors (FPSs) can decrease considerably owing to environmental factors and parasitic capacitance. In order to overcome this limitation, this paper proposes a highly-sensitive 300 dpi mutual-capacitive transparent fingerprint sensor (FPS) with uniquely designed reference lines for device security. Specifically, the reference lines of the FPS induce capacitance cancellation. Images of fingertips under dry, wet, and oily surface conditions were obtained in the presence and absence of the reference lines. The results showed that the fingerprints were significantly distorted in anomalous surface environments when the reference lines were not used. However, when the reference lines were used, the sensitivity improved irrespective of the environmental conditions. With the edge-detection processing, the proposed FPS exhibited 9.25 %, 61.49 %, and 8.60 % increase in the ridge sensing improvement (RSI) of dry, oil, and wet condition, respectively, thus significantly enhancing the sensing capability. Therefore, we believe the proposed FPS can increase device security owing to its excellent performance.**

***Index Terms*— Highly-sensitive, transparent, mutual-capacitive, fingerprint sensor, reference lines.**

I. Introduction

GIVEN that personal information security has consistently grown in the Internet of Things (IoT) era, biometric identification technologies have gained extensive attention owing to the rapid advancement of information technology platforms [1], [2]. A human fingerprint contains ridges and valleys and has been extensively used as a biometric identifier owing to its excellent reliability and sensitivity. Among different sensors, the mutual-capacitive-type fingerprint sensor (FPS) does not entail ghost signals and exhibits multi-touch capabilities owing to individually measured intersections; this allows the implementation of a FPS whose multiple pixels are concurrently contacted [3], [4], [5], [6], [7], [8].

At present, it is necessary to deploy FPSs based on a transparent substrate at wide-ranging frequencies to increase functionality and maintain the appearance of devices [5], [9]. However, owing to the significant sheet resistance of transparent electrodes, a typical mutual-capacitive FPS possesses a parasitic capacitance higher than the actual sensing capacitance, especially in flexible FPSs. Additionally, the quality of the acquired fingerprint images decreases owing to environmental factors, thereby resulting in contact failure and differences in sensitivity [5], [6], [7]. Therefore, it is essential to develop a FPS model framework that not only exhibits excellent sensitivity, especially the ridge detection due to the increase of the ridge-valley contrast, but sustains a good response under different operational situations while maintaining high transparency.

In this paper, we propose a novel high-fill-factor mutual-capacitive FPS model by introducing an additional reference pixel module for base capacitance cancellation. These reference lines enable the sensor to directly detect and extract capacitive changes between the reference and sensing cells, which exclude base capacitance value and improve the output signal visualization. Furthermore, we investigate the performance and reliability of the proposed sensor based on different skin conditions and their influence on the output.

II. Experiment

Fig. 1. (a) shows the layout of the proposed mutual-capacitance FPS. Each fundamental component comprised opaque line-pattern Mo layers [not shown in Fig. 1. (a)], SiO_2 insulators owing to create high capacitance value variations between ridges and valleys, transparent indium tin oxide (ITO) sensing electrodes, and overlaid Al_2O_3 layers.

First, a 150 nm ITO layer was coated on as a sensing electrode to ensure transparency. A 200 nm Mo film was deposited onto a glass substrate and patterned into transmitter (T_x) line

Manuscript received 30 August 2022; revised 15 September 2022; accepted 18 September 2022. Date of publication 22 September 2022; date of current version 24 October 2022. This work was supported by the Industry Technology Research and Development Program through the Ministry of Trade, Industry, and Energy (MOTIE), South Korea, under Grant 20006467. The review of this letter was arranged by Editor S. Zhang. *(Junghoon Yang and Yeon-Wha Oh contributed equally to this work.) (Corresponding authors: Il-Suk Kang; Sang-Hee Ko Park.)*

Junghoon Yang, Sarawut Siracosit, Hyunwoo Park, Guk-Jin Jeon, and Sang-Hee Ko Park are with the Department of Materials Science and Engineering, Korea Advanced Institute of Science and Technology (KAIST), Yuseong-gu, Daejeon 34141, Republic of Korea (e-mail: shkp@kaist.ac.kr).

Yeon-Wha Oh, Sang-Hee Jung, and Il-Suk Kang are with the National NanoFab Center (NNFC), Yuseong-gu, Daejeon 34141, Republic of Korea (e-mail: iskang@nnfc.re.kr).

Jungmoo Lee and Sang Gyun Kim are with the GRIT Custom-Integrated Chip (GRIT CIC), Nowon-gu, Seoul 01886, Republic of Korea.

Hanbyul Kim and Kyunghak Lee are with the Wireless Recharge RF Power Solution (WARPS), Seongdong-gu, Seoul 04782, Republic of Korea.

Jae-Hyun Ahn is with the Medical Credible Guardian (AMCG), Seocho-gu, Seoul 06605, Republic of Korea.

Color versions of one or more figures in this letter are available at https://doi.org/10.1109/LED.2022.3208560.

Digital Object Identifier 10.1109/LED.2022.3208560

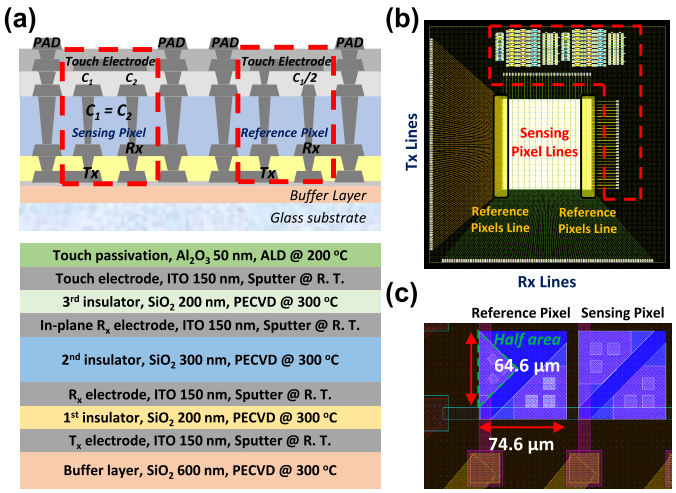

Fig. 1. (a) Mutual FPS cross-section layout and (b) 300 dpi FPS-array layout with testing pads. The sensor area comprises 91 T_x and 90 R_x lines with the reference pixels lines in the first and the last columns, resulting 91 x 88 (8,008) pixels in total. (c) Two unit cells (left: reference pixel, right: sensing pixel) comprising both T_x and R_x lines (top view).

via a lift-off process. Then, the first insulator of the 200 nm SiO_2 layer was deposited, resulting in the formation of a dry-etched via-hole pattern. The same procedure was applied for depositing the second 300 nm SiO_2 inter-dielectric layer for the receiver (R_x) line. To form a stable capacitance with the top layer touching the electrode, a third layer with 150 nm and 200 nm thick ITO and SiO_2 layers, respectively, was deposited, in which the via pattern was established in the reference pixel. Finally, before depositing Mo as contact pads, a 50 nm Al_2O_3 overlaid layer was deposited and patterned to avoid mechanical breakdown and withstand ambient environments [10].

Throughout the fabrication process, each inspection, including image cross-section and element mapping, was performed using FIB (Dual Beam FIB; FEI NOVA 200), SEM (FE-SEM; Hitachi SU 8100), and EDS mapping (FE-TEM; Tecnai G^2 F30 S-Twin). By inputting voltage pulses of 15 V, 50 kHz in T_x lines, the original fingerprint images were acquired in the low-frequency region of the system from the analog R_x output signal of the connected ROIC. The output was then processed via 2D mapping using a four-fold integration (40 μ s) under three skin conditions–dry, wet, and oiled–to investigate the influence of the surface on the degradation of the images. The Canny edge detection is applied using MATLAB with the Gaussian filter to remove non-uniformity from the image by smoothening, particularly in helping enhance the image quality and image recognition. The image gradient is then computed to determine the frequency at the high spatial derivatives regions: ridges and valleys of detected fingerprints. Subsequently, the non-maximum suppression is performed to remain only the pixels with the maximum values in edges [11].

III. Results and Discussion

Fig. 1. (c) shows the unit cell of the sensing and reference pixels. The mutual-capacitance FPS operates according to the potential difference between two conductive T_x and R_x at the sensing pixel to detect the difference between the ridge (C_{ridge}) and valley (C_{valley}) capacitance ($C_{ridge\text{-}valley}$, sub-fF level) [12]. By applying logic pulses to the T_x lines, which operate as the driving electrode, an electric field is generated between the sensing electrode and T_x, thereby forming a baseline mutual capacitor (C_m). The R_x lines function as the sensing electrode and collect a majority of the coupled charges from the touch electrode to generate a second C_m. These charges are further amplified and transformed into a voltage level using a readout integrated circuit (ROIC) [13], [14]. The field coupling at the edge of the touch electrode is attenuated in the presence of the fingertip [4], [15], [16]. At the reference pixel, the R_x electrode area capacitance was 0.5 C_m, which was equal to the total combination of the mutual capacitor of the T_x and R_x regions, as shown in Fig. 1. (c). The T_x electrode was connected to the touch electrode through holes, thereby causing the reference capacitance (C_{ref}) to be fixed, regardless of the presence of the fingertip. The FPS touch screen panel structure comprised a crossline structure with a large plate area and a mutual capacitance of the panel to maximize the fill factor (50 %) and improve touch detection, respectively [8], [15], [16], [17].

The capacitor value read from the FPS, which is same as the size of the output signal, varied depending on the presence or absence of the fingerprint. Without applying the reference electrodes, the differences in the output signal at the ridge and valley were low compared to the base signal owing to the presence of a high parasitic capacitor. However, in the absence of the fingerprint, when the reference electrodes were ON, the AC signal presented the same magnitude at the inputs of both ends of the analog comparator, considering the total capacities of the (T_x, R_x) and reference lines were the same, thereby resulting in a zero comparator output (self-calibration). When the finger was placed on the panel, the signal appeared at a different magnitude in the sensing and reference regions, while the unchanged base signal was ignored. Therefore, turning the reference electrode can make the output signal from the sensing ridge and valley more prominent via base capacitance cancellation, thereby increasing the overall sensing capacity, specifically ridge region detection.

The fingerprint data was initially obtained without operating the reference electrode. As shown in Fig. 2(a), (c), (e), the low contrast between the ridges and valleys indicates poor fingerprint detection visibility for all surface conditions. Owing to the difficulty in capturing clear and low-noise images, the fingerprint pattern generated from the oily fingertip [Fig. 2(c)] exhibited low clarity and was difficult to identify compared to the pattern from the dry [Fig. 2(a)] and wet conditions [Fig. 2(e)]. Furthermore, edge detection loss can also be depicted in certain parts of the images, especially in the core, the uppermost inner ridge region, in the presence of oil layer. As grease can overpower ridge characteristic, the result, as shown in Fig. 2(c), shows it diminished the sensing area and characteristics of the valleys. Moreover, this core absence reduces not only the detectability of ridge frequency, but also the functionality of other security detection techniques, e.g., core point profile or location detection [18], [19], [20].

The results of the subsequent operation of the FPS employing reference lines are shown in Fig. 2(b), (d), (f). Despite short integration time, the original fingerprint images were well obtained under all environmental circumstances

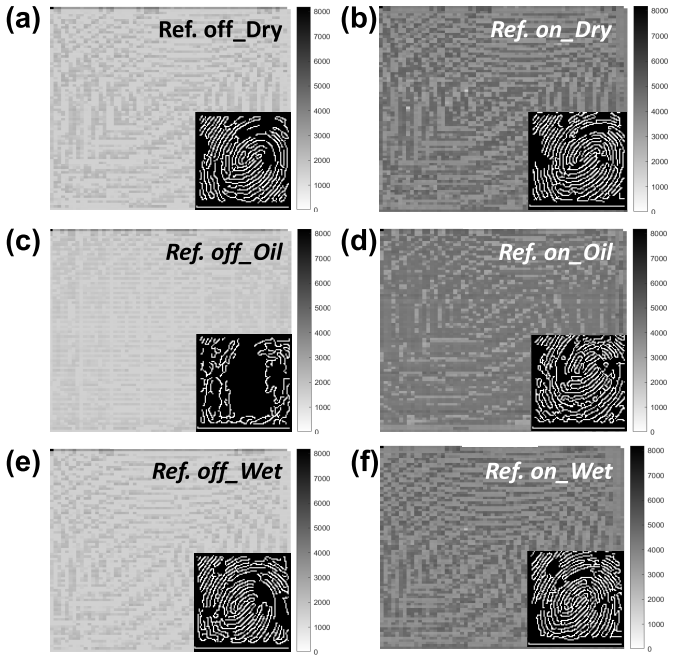

Fig. 2. Fingerprint images obtained under (a, b) dry, (c, d) oil, and (e, f) wet conditions. Each condition is operated (a, c, e) without and (b, d, f) with reference electrodes. Each figure is attached with an edge-detection processing version using the Canny method.

TABLE I
COMPARISON OF THE RIDGE FREQUENCY IN EDGE-DETECTION PROCESSING FINGERPRINT IMAGES BASED ON THE SKIN CONDITION AND THE REFERENCE ELECTRODE OPERATION IN THE FPS

Condition	Valley Frequency (count)	Ridge Frequency (count)	Ridge Sensing Improvement (RSI) (%)
Ref. off_Dry	5,976	2,032	9.25
Ref. on_Dry	5,779	2,229	
Ref. off_Oil	6,848	1,160	61.49
Ref. on_Oil	5,818	2,190	
Ref. off_Wet	5,905	2,103	8.60
Ref. on_Wet	5,716	2,292	
Total Frequency = 8,008			

with improved area resolution and qualitatively demonstrated through differences in the ridge-valley contrast. In addition, the edge-detection images visibly show a significant improvement in the amount of detected ridge frequency compared to that of the non-operating reference electrode. To quantitatively compare the increment of the ridge sensitivity, the ridge sensing improvement (RSI) was obtained as

$$\mathrm{RSI} = \frac{f(\mathrm{ridge})_{\mathrm{on}} - f(\mathrm{ridge})_{\mathrm{off}}}{\overline{f(\mathrm{ridge})}} \times 100\ \% \qquad (1)$$

where $f(\mathrm{ridge})_{\mathrm{on}}$ and $f(\mathrm{ridge})_{\mathrm{off}}$ are ridge frequency detected in the edge-detection process images in reference electrode ON and OFF conditions, respectively, and $\overline{f(\mathrm{ridge})}$ represents the average value of ridge frequency in both conditions. Using Eq.(1), the RSI of each condition was calculated as shown in Table. I, including the ridge and valley frequencies. When the reference pixels were solely operated, the RSI values increased under every operating condition by at most 65 % compared to regular operation, thereby indicating that the performance of proposed FPS was not attributable to surface conditions but

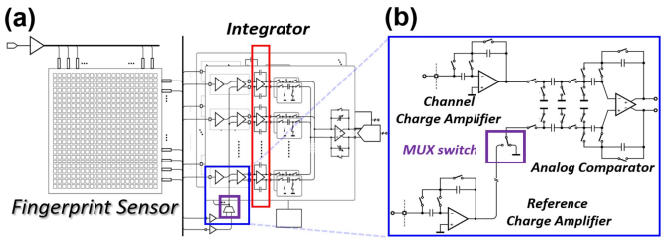

Fig. 3. (a) Fingerprint ROIC (readout integrated circuit) architecture, comprising Analog front-end architecture (blue box) and integrator (red box), and (b) Analog front-end architecture, comprising channel and reference charge amplifiers, the analog comparator, and MUX switch (purple box) for controlling reference pixels.

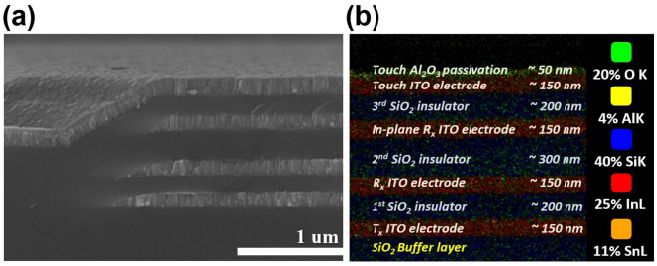

Fig. 4. (a) FIB-SEM and (b) EDS cross section mapping of the fabricated mutual-capacitive FPS with respective thickness.

rather to signal enhancement via base capacitance cancellation caused by the activation of reference pixels.

According to the designed analog front-end and the FPS ROIC architectures illustrating in Fig. 3, owing to the minimal capacitance differential between the ridge and valley, the circuit noise must be controlled at a superficial level. As such, low-frequency noise such as flicker noise (1/f), which can cause a DC offset problem, is preferred for avoiding at the analog circuit level [21]. Therefore, for a low-noise FPS ROIC architecture, the charge amplifier (CA) uses an offset sampling capacitor to reject the DC offset owing to the non-ideal characteristics of the operational amplifier. Considering that the raw data values were relatively constant, no further calibration was required from the ROIC and external analysis programs. Furthermore, to validate that each layer was well-deposited, FIB and SEM analyses were performed to observe the cross-section of the FPS (Fig. 4). The results showed that the FPS had a distinct interface between each layer, and all layers were accurately deposited to the specified thickness.

IV. CONCLUSION

This study achieved a sufficient performance level for transparent fingerprint sensors compared to conventional non-transparent sensors. By introducing additional base-capacitance-canceling reference electrodes to the mutual-capacitive layout, we achieved improved ridge sensitivity. Further analyses showed that the fabricated sensor could withstand various surface environments while improving the output signal resolution even at low integration times. We believe the proposed FPS can be further developed on flexible transparent substrate sensors for applications in electronics and identification.

REFERENCES

[1] W. Yang, S. Wang, N. M. Sahri, N. M. Karie, M. Ahmed, and C. Valli, "Biometrics for Internet-of-Things security: A review," *Sensors*, vol. 21, no. 18, p. 6163, Sep. 2021, doi: 10.3390/s21186163.

[2] K.-S. Kim and D. U. Kim, "Overview on smart sensor technology for biometrics in IoT era," *J. Microelectron. Packag. Soc.*, vol. 23, no. 2, pp. 29–35, Jun. 2016, doi: 10.6117/kmeps.2016.23.2.029.

[3] G. Barrett and R. Omote, "Projected-capacitive touch technology," *Inf. Display*, vol. 26, no. 3, pp. 16–21, Mar. 2010, doi: 10.1002/j.2637-496X.2010.tb00229.x.

[4] S. Heo, "Design of touch screen controller ic for transparent fingerprint sensor," Ph.D. dissertation, Ulsan Nat. Inst. Sci. Technol. (UNIST), Ulsan, South Korea, Dec. 2017.

[5] H. Ma, Z. Liu, S. Heo, J. Lee, K. Na, H. B. Jin, S. Jung, K. Park, J. J. Kim, and F. Bien, "On-display transparent half-diamond pattern capacitive fingerprint sensor compatible with amoled display," *IEEE Sensors J.*, vol. 16, no. 22, pp. 8124–8131, Nov. 2016, doi: 10.1109/JSEN.2016.2605125.

[6] H. Hwang, H. Lee, M. Han, H. Kim, and Y. Chae, "A 1.8-V 6.9-mW 120-fps 50-channel capacitive touch readout with current conveyor AFE and current-driven $\delta\sigma$ ADC," *IEEE J. Solid-State Circuits*, vol. 53, no. 1, pp. 204–218, Jan. 2018, doi: 10.1109/JSSC.2017.2750326.

[7] H. Hwang, H. Lee, B. Jang, H. Kim, T. Lee, and Y. Chae, "56–3: A 500-dpi transparent on-glass capacitive fingerprint sensor," in *SID Symp. Dig. Tech. Papers*, vol. 48, no. 1. Hoboken, NJ, USA: Wiley, May 2017, pp. 838–841, doi: 10.1002/sdtp.11781.

[8] S.-L. Huang, S.-Y. Hung, and C.-P. Chen, "Frequency hopping and parallel driving with random delay especially suitable for the charger noise problem in mutual-capacitive touch applications," *IEEE Access*, vol. 7, pp. 3980–3993, 2019, doi: 10.1109/ACCESS.2018.2888927.

[9] B. W. An, S. Heo, S. Ji, F. Bien, and J.-U. Park, "Transparent and flexible fingerprint sensor array with multiplexed detection of tactile pressure and skin temperature," *Nature Commun.*, vol. 9, no. 1, pp. 1–10, Jul. 2018, doi: 10.1038/s41467-018-04906-1.

[10] B. Nalcaci and M. P. Gonullu, "Insight of mechanical and morphological properties of ALD-Al_2O_3 films in point of structural properties," *Appl. Phys. A, Solids Surf.*, vol. 127, no. 6, pp. 1–10, May 2021, doi: 10.1007/s00339-021-04601-x.

[11] R. Chanklan, K. Chaiyakhan, A. Hirunyawanakul, K. Kerdprasop, and N. Kerdprasop, "Fingerprint recognition with edge detection and dimensionality reduction techniques," in *Proc. 3rd Int. Conf. Ind. Appl. Eng.*, Nakhon Ratchasima, Thailand, Jan. 2015, pp. 1–6, doi: 10.12792/ICIAE2015.098.

[12] H. Cummins and C. Midlo, *Finger Prints, Palms and Soles: An Introduction to Dermatoglyphics*, vol. 319. New York, NY, USA: Dover, 1961, doi: 10.1016/B978-0-7506-7844-5.X5109-1.

[13] M.-J. Soh and S.-Y. Soh, "Readout integrated circuit for dynamic imaging," U.S. Patent 13 584 885, Feb. 20, 2014.

[14] W. Seo, J.-E. Pi, S. H. Cho, S.-Y. Kang, S.-D. Ahn, C.-S. Hwang, H.-S. Jeon, J.-U. Kim, and M. Lee, "Transparent fingerprint sensor system for large flat panel display," *Sensors*, vol. 18, no. 1, p. 293, Jan. 2018, doi: 10.3390/s18010293.

[15] H.-J. Kim-Lee, S. W. Hong, D. K. Kim, J. Kim, H. S. Kim, S.-W. Chung, E.-H. Cho, H.-S. Kim, and B.-K. Lee, "On-screen fingerprint sensor with optically and electrically tailored transparent electrode patterns for use on high-resolution mobile displays," *Microsyst. Nanoeng.*, vol. 6, no. 1, pp. 1–12, Nov. 2020, doi: 10.1038/s41378-020-00203-4.

[16] Z. Ye, M. Wong, M.-T. Ng, K.-H. Chui, C.-K. Kong, L. Lu, T. Liu, and J. K. Luo, "High precision active-matrix self-capacitive touch panel based on fluorinated ZnO thin-film transistor," *J. Display Technol.*, vol. 11, no. 1, pp. 22–29, Jan. 2015, doi: 10.1109/JDT.2014.2357845.

[17] J.-S. An, S.-H. Han, and J.-H. Ye, "A sensing mode reconfigurable analog front-end IC for capacitive touch and a-IGZO TFT-based active-matrix capacitive fingerprint sensors," *IEEE Sensors J.*, vol. 19, no. 23, pp. 11544–11552, Dec. 2019, doi: 10.1109/JSEN.2019.2935231.

[18] M. A. Olsen, M. Dusio, and C. Busch, "Fingerprint skin moisture impact on biometric performance," in *Proc. 3rd Int. Workshop Biometrics Forensics (IWBF)*, Mar. 2015, pp. 1–6, doi: 10.1109/iwbf.2015.7110223.

[19] V. Kumari, M. K. Thakar, B. Mondal, and S. K. Pal, "Effects of oils, lotions, hand sanitizers, and mehendi on fingerprints captured through digital fingerprint scanner," *Egyptian J. Forensic Sci.*, vol. 11, no. 1, pp. 1–7, May 2021, doi: 10.1186/s41935-021-00222-w.

[20] F. Belhadj, "Biometric system for identification and authentication," Ph.D. dissertation, Ecole Nationale Supérieure en Informatique Alger, Oued Smar, Algeria, Feb. 2017, doi: 10.12792/ICIAE2015.098.

[21] W. Jung, *Op Amp Applications Handbook*. London, U.K.: Newnes, 2005, doi: 10.1002/ajpa.1330020212.